Validation of ASCE 41-13 Modeling Parameters and Acceptance Criteria for Rocking Shallow Foundations

Manouchehr Hakhamaneshi,[a] **M.EERI, Bruce L. Kutter,**[a] **M.EERI, Mark Moore,**[b] **M.EERI, and Casey Champion,**[b] **M.EERI**

The standard ASCE 41-13 *Seismic Evaluation and Retrofit of Existing Buildings* includes new provisions for linear and non-linear modeling parameters and acceptance criteria for rocking shallow foundations. The new modeling parameters and acceptance criteria were largely based on model tests on rectangular rocking foundations with a limited range of footing length to width ratio (L/B). New model test results are presented, including a systematic variation of L/B and also non-rectangular (I-shaped) footings. This new data along with previously published results are presented to validate the trilinear modeling parameters and acceptance criteria of ASCE 41-13. This paper investigates the effects of footing shape on the residual settlement, residual uplift, rocking stiffness, and re-centering. Overall, the new data supports the provisions of ASCE 41-13; however, the acceptance limits for rocking rotation of I-shaped footings could be reduced to produce performance consistent with the acceptance limits for rectangular footings. [DOI: 10.1193/121914EQS216M]

BACKGROUND ON ASCE 41

ASCE 41-13 is an update and combination of the ASCE 41-06 and ASCE 31-03 standards, which are intended for the seismic evaluation and retrofit of existing buildings. ASCE 41-13 establishes tables of acceptance criteria for different building performance levels to implement performance-based design for different levels of earthquake intensity. The structural performance levels may vary for different seismic hazard levels. The typical performance levels used in the standard are immediate occupancy (IO), life safety (LS), and collapse prevention (CP). ASCE 41-13 provides new modeling parameters and acceptance criteria for rocking foundations in Chapter 8 with component action tables similar to other material chapters. The modeling parameters provide the means to approximate the shape of the backbone curve for the moment-rotation behavior using a trilinear model. The provided acceptance criteria are presented as values of maximum acceptable rotation demand for the IO, LS, and CP performance levels.

The rationale for the determination of the modeling parameters and acceptance criteria is described in detail by Kutter et al. (2016). At the time of development of the now published ASCE 41-13 standard, there was strong evidence that footing shape had a significant effect

[a] Dept. of Civil & Environ. Engrg., UC Davis. 1 Shields Ave, Davis, CA 95616. mhakhamaneshi@ucdavis.edu, blkutter@ucdavis.edu
[b] ZFA Structural Engineers, SE, LEED AP, markm@zfa.com, caseyc@zfa.com

on the performance of rocking foundations. Subsequently, a more extensive series of model tests investigating the effect of footing shape and embedment has been completed by Hakhamaneshi and Kutter (2016). The new results include the first ever rocking foundation model tests with a systematic variation in shape of embedded and surface rectangular footings and I-shaped footings. This paper uses the data from this new series of tests as an independent validation of the proposed modeling parameters and acceptance criteria for rocking foundations provided in ASCE 41-13.

ROCKING FOUNDATIONS

Figure 1a shows a rocking foundation with length (L), width (B) and area ($A = B \cdot L$), which is subject to a vertical load (P), and a horizontal load (V) applied at a lever arm height (h_v) above the base of the footing. These loads, due to seismic and gravity forces, can cause the footing to rotate, slide and settle. The soil exerts a resultant force on the footing, which consists of a sliding resistance force and a normal force. For a surface footing on a rigid frictional interface, the sliding is expected to occur prior to rocking if the applied horizontal force is equal to the sliding resistance of the footing and the applied moment ($M = V \cdot h_v$) is smaller than the resisting moment ($PL/2$). On the other hand, if the horizontal load is applied at a height greater than $L/(2\mu)$ (where μ is the coefficient of friction), then the footing will tip about its edge. For soil that is not rigid relative to the footing, the footing does not bear on the sharp edge as it rocks. Instead, a minimum critical contact area, A_c, is required to support the vertical loads. The moving of the contacting area results in a curved interface, with localized bearing failure (Gajan and Kutter 2008). As shown in Figure 1a, the critical contact area along one edge of the footing will dig into the soil below while the other edge of the footing separates (uplifts) from the soil creating a gap between the footing and the soil. If the lateral load, V, is removed, the vertical load, P, causes gap closure and thus provides a natural self-centering response.

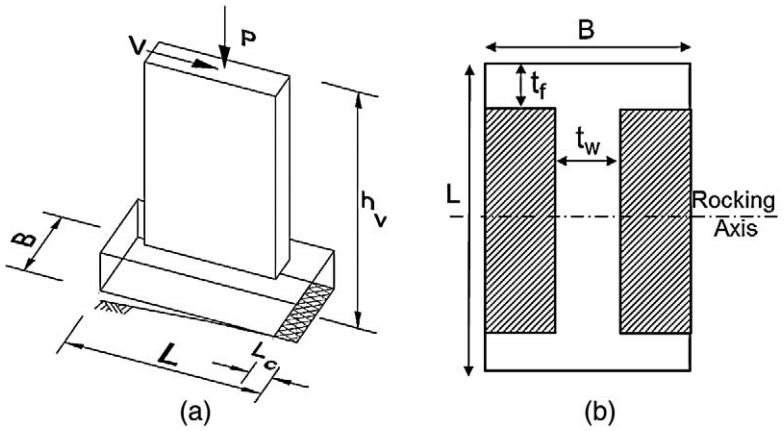

Figure 1. (a) Rocking shallow foundation under vertical load (P), lateral load (V) with definition of critical contact length ($L_c = A_c/B$), (b) Footing shape parameters for rectangular and I-shaped footings.

For rectangular footings loaded along the length of the footing, the critical contact length, L_c, is directly related to the critical contact area: $L_c = A_c/B$. The value of A_c represents the minimum area of the footing required to support the vertical load when the soil's ultimate bearing capacity (q_{ult}) is fully mobilized on the contact area and $A_c = P/q_{ult}$. Gajan and Kutter (2008) described the difference between A/A_c and the factor of safety with respect to bearing capacity, including the effects of soil type, footing shape factors and the size of the footing. Deng and Kutter (2012b) describe the iterative process required to calculate A_c since q_{ult} is sensitive to A_c. The notation for critical contact area ratio (ρ_{ac}) is used in ASCE 41-13 to denote the ratio of A_c to the total area of the footing, A, as shown in Equation 1:

$$\rho_{ac} \equiv \frac{A_c}{A} \tag{1}$$

Similar to previous standards, the moment capacity of a rectangular rocking footing in ASCE 41-13 is calculated from:

$$M_{c\text{-}foot} = \frac{PL}{2}(1 - \rho_{ac}) \tag{2}$$

In this equation, P is the total vertical load acting on the footing due to gravity (including the superstructure weight, overburden and footing weight) as well as seismic loads from transient overturning action, and L is the in-plane length of the footing (perpendicular to the rocking axis). Others (e.g., Allotey and El Naggar 2003 and Meyerhof 1963) have produced similar equations for the rocking moment capacity but with ρ_{ac} replaced with $1/FS_p$, the factor of safety with respect to concentric vertical loading. As the term factor of safety brings to mind outdated concepts of working stress design philosophy and because the inverse of A_c/A is not clearly correlated to safety, we dispense with the FS_p terminology in favor of the critical contact area ratio, ρ_{ac}. The rocking moment capacity can also be represented as shown in Equation 3:

$$M_{c\text{-}foot} = \frac{PL}{2}\left(1 - \frac{q}{q_c}\right) \tag{3}$$

In this equation q is the vertical bearing pressure if P is distributed uniformly ($q = (P/BL)$) and q_c is the expected bearing capacity of the critical contact area. The ratio of q/q_c is also equal to ρ_{ac}:

$$\frac{q}{q_c} = \frac{P/BL}{P/A_c} = \frac{A_c}{A} = \rho_{ac} \tag{4}$$

However, it should be pointed out that bearing capacity, q_c, depends on the shape of the loaded critical contact area. Since the shape of the critical contact area during rocking on one edge is not the same as the shape of the overall footing, the ratio q/q_c will not be equal to $1/FS_p$.

NONLINEAR MODELING OF A BUILDING SYSTEM

A model of a building using nonlinear static or nonlinear dynamic procedures in ASCE 41-13 includes many nonlinear component actions (e.g., beams, columns and foundations). The behavior of each component is represented using modeling parameters listed in their corresponding component action table. The proposed models for individual components in the standard provide the user with the necessary tools to reasonably model the stiffness, strength and strength degradation. Component action tables also provide the deformation capacity used to determine the acceptance criteria for the corresponding component.

The standard allows three methods for analyzing rocking foundations. In Method 1, uncoupled moment, shear and axial springs (Figure 2c) are used to model the rigid, rocking footing; if the vertical load, P, on the footings is dependent on the rotation due to frame action, iteration may be required to find the appropriate P including seismic contributions. For Method 1, the vertical and shear springs are bilinear (elastic, perfectly plastic) but a tri-linear relationship is specified for the moment-rotation relationship (line AFBC in Figure 2b). ASCE 41-13 does not provide modeling parameters for unloading of the footing (line CZ), and guidance on the unloading slope can be found in Deng et al. (2014).

In Method 2 (ASCE 2013, Kutter et al. 2016), a rocking footing is modeled by using discrete nonlinear gapping foundation springs distributed along the soil-footing interface; Method 2 adequately accounts for the coupled effect of axial loading on moment capacity, however, no coupling between the moment and shear behavior is accounted for. Method 2 can be used to capture hysteretic damping and the re-centering effects on footings, and thus it

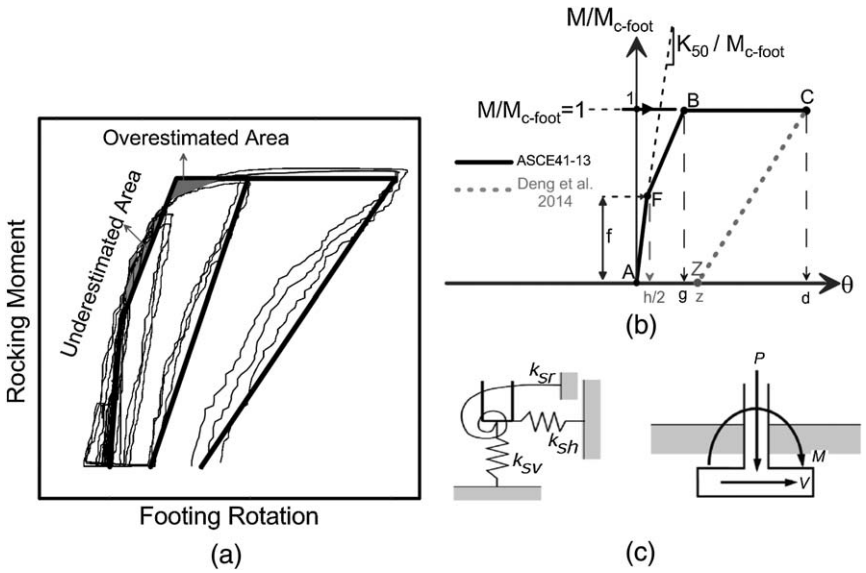

Figure 2. (a) Demonstration of areas overestimated and underestimated in fitting a curve to the experimental data, (b) the proposed trilinear backbone curve for rocking foundations, and (c) uncoupled horizontal, vertical, and rotational springs.

may be useful for nonlinear dynamic analysis procedures. Lastly, Method 3 is used when the concrete footing is assumed to be deformable relative to the foundation soil (i.e., a relatively thin elastically flexible footing or a footing in which a plastic hinge forms in the concrete).

NONLINEAR STATIC PROCEDURES USING METHOD 1

For the nonlinear static procedure, the seismic load is applied to the system as an equivalent distributed static lateral load. The resulting target displacements are applied for different seismic loads until a pushover curve is obtained. The pushover curve plots the relation between the seismic load and the expected displacements. The global response of the system is captured by using the modeling parameters of each building component action, including the foundation spring elements. After the system reaches the target displacement, the demand on each component of the building is compared to the acceptance criteria for that particular component. The uncoupled axial, shear and rotational (moment) springs for Method 1 (Figure 2c) are based on the modeling parameters specified in ASCE 41-13, excerpts of which are included in Kutter et al. (2016). The columns in this component action table identify footing shape parameters and the corresponding modeling parameters and acceptance criteria. The footing shape parameters are b/L_c, $(A_{rect} - A)/A_{rect}$ and A_c/A. The parameter b/L_c accounts for the shape of the rocking footing's critical contact area, and for rectangular footings $b = B$, where B is the width of the rocking foundation parallel to the axis of rocking and L_c is the critical contact length (Figure 1a). For an I-shaped footing, $b = t_f$, where t_f is the thickness of the flange. The "missing area ratio" (or MAR) is defined as $(A_{rect} - A)/A_{rect}$. As shown in Figure 1b, for an I-shaped footing, the missing area ratio is the difference between the area of the circumscribed rectangle and the area of the footing divided by the area of the circumscribed rectangle. For a rectangular footing, $MAR = 0$, and for an I-shaped footing with infinitesimally small web and flanges, $MAR = 1$.

As shown in Figure 2b, a trilinear backbone curve (dark lines connecting AFBC) is used to represent the moment-rotation behavior of the rotational spring elements. Figure 2b plots the moment demand normalized by the rocking moment capacity ($M/M_{c\text{-}foot}$) versus the footing rotation where, for a rectangular footing, the rocking moment capacity is calculated using Equation 2 or 3. For any other footing shapes, the rocking moment capacity can be calculated by multiplying the axial load by the moment lever-arm between the centroid of the footing and the centroid of the critical contact area. For large deformations, the analysis must also account for P-Δ effects that would contribute to the moment about the centroid of the base of the footing. Modeling parameters in the component action table (Kutter et al. 2016, ASCE 2013) include three parameters g, d, and f that are used to define the backbone curve. As illustrated in Figure 2b, the parameters g and d reflect rotation angles and f is a unitless parameter known as the elastic strength ratio. These parameters are presented as a function of the footing shape parameters and linear interpolation between the numerical values is permitted. The basis for setting the modeling parameters and acceptance criteria in ASCE 41-13 is described by Kutter et al. (2016). The parameter f is defined as the normalized moment at the first change in rotational stiffness in the trilinear relationship. Johnson (2012) studied the data from 14 researchers and suggested that a value of $f = 0.5$ provides a reasonable fit to the data set. The next modeling parameter, g, is the footing rotation required to mobilize the rocking moment capacity (point B in Figure 2b). The corresponding moment capacity, $M_{c\text{-}foot}$, was obtained using Equation 2 and the parameter g was obtained by

overlying the trilinear model on experimental moment-rotation data as proposed by Johnson (2012). Figure 2a illustrates Johnson's technique where the area of the hysteretic loops over the trilinear model along the FB line was forced to be equal to the area under the backbone curve upon reaching parameter g. Lastly, the parameter d represents the maximum footing rotation. The resultant backbone curve in ASCE 41-13 is shown as segments AFBC (thick solid lines) in Figure 2b. For the I-shaped footings, the allowable rotation decreases as the MAR increases. For rectangular footings, the allowable rotation decreases as b/L_c decreases.

The backbone curve allows one to perform a monotonic pushover analysis for a nonlinear static procedure. This backbone curve may also be applicable to nonlinear dynamic procedures (NDP) if hysteretic damping, re-centering and pinching are taken into account. Deng et al. (2014) recommended relationships for the unloading, along the dashed CZ line. The test results presented below are used to validate the re-centering parameter (z) and the hysteresis loops proposed by Deng et al. (2014) that were used to determine the ASCE 41-13 parameters f, g, and d. ASCE 41-13 provisions for rocking foundation are limited to rocking-dominated footings, for which sliding deformations are small and the moment capacity is not significantly reduced by the presence of the lateral shear force on the footing. Gajan and Kutter (2008) and Hakhamaneshi (2014) showed that if the footing's $M/(V \cdot L)$ ratio is greater than one, that rocking (as opposed to sliding) controls. Based upon this, ASCE 41-13 component action tables are limited to cases with $M/(V \cdot L) > 1$; the standard currently does not provide modeling parameters nor acceptance criteria for sliding dominated footings.

TESTING PROGRAM

Johnson (2012), Deng and Kutter (2012b), Anastasopoulos et al. (2010), Gajan and Kutter (2008) and others have performed experiments to determine moment-rotation behavior of shallow foundations. A new series of slow cyclic tests were conducted to systematically evaluate the effects of footing shape on the moment-rotation behavior. The frequency of the load cycles was less than about 0.01 cycles per second prototype scale. Hence, the accelerations associated with rocking were less than 0.0001 g (prototype scale) and inertia forces are considered negligible. Gajan and Kutter (2008) reported that ground shaking causes a reduction in the moment capacity of 15–25% for $1/15 < \rho_{ac} < 1/2$ and different levels of shaking. Deng et al. (2012a), Hakhamaneshi et al. (2012), and Hakhamaneshi (2014) summarized results of experiments with maximum cyclic rotation up to 5% and cumulative footing rotation up to 30%. Results showed that settlements of footings with similar ρ_{ac} fall in boundaries consistent for different types of loading and soil environments.

The tests were performed at the Center for Geotechnical Modeling at UC Davis using the 1 m radius (Schaevitz) centrifuge. Sixteen different soil-foundation-superstructure models listed in Table 1 (eight embedded and eight surface footings) were tested at a centrifugal acceleration of 35 g. The slow cyclic load was applied horizontally to a stiff shear-wall structure attached to the footings. A combination of vertical and horizontal Linear Potentiometers and MEMS accelerometers were used to capture displacements and rotations of the footing and shear wall. ASCE 41-13 provisions permit the derivation of modeling parameters and acceptance criteria using experimentally obtained cyclic response characteristics of a component. Since a specific testing protocol is not recommended in ASCE 41 and is often

Table 1. Footing properties in model scale. The length scale factor to convert results to prototype scale is 35.

Test Name	L (mm)	B (mm)	t_w (mm)	t_f (mm)	b (mm)	D (mm)	A_c/A	P (N)
1.4_e_R_0.6	150	90			90	32	0.114	2841
1.45_e_R_1.55	110	170			170	32	0.115	3910
1.57_e_R_0.14	210	30			30	32	0.102	1435
1.5_e_I50_0.11	150	75	26	17	17	32	0.098	1209
1.5_e_I50_0.17	150	75	19.5	25	25	32	0.105	1209
1.5_e_I35_0.13	150	75	39	20	20	32	0.109	1535
1.5_e_I35_0.26	150	75	20	39	39	32	0.109	1535
1.5_e_I65_0.09	150	75	16	13	13	32	0.090	834
2_s_R_1.55	110	170			170	0	0.250	3941
1.6_s_R_0.14	210	30			30	0	0.233	1341
1.4_s_R_0.6	150	90			90	0	0.244	2841
1.5_s_I35_0.26	150	75	20	39	39	0	0.286	1535
1.5_s_I35_0.13	150	75	39	20	20	0	0.294	1535
1.5_s_I50_0.17	150	75	19.5	25	25	0	0.323	1170
1.5_s_I50_0.11	150	75	26	17	17	0	0.323	1209
1.5_s_I65_0.09	150	75	16	13	13	0	0.385	826

dependent on the component being tested, a loading protocol consistent with the general guidelines of FEMA P-795 was developed and is also explained by Liu et al. (2014). FEMA P-795 prescribes cyclic-load testing protocols and states that "the deformation history should be described in terms of a well-defined quantity (e.g., displacement, story drift rotation) and should consist of symmetric deformation cycles of step-wise increasing amplitude" (ATC 2011, pp. 50–51). Starting with cyclic displacements equal to 0.1% of the height of the actuator above the base of the footing, three cycles of displacement were applied. Then, the amplitude of applied displacement was doubled, three more cycles applied, etc., until the amplitude of displacement was 6% of the height of the actuator above the base of the footing. Since the test models were rocking dominated, the footing rotation was approximately equal to displacement/height and the maximum rotation was approximately 6%. All the rotations reported in this paper are reported as the tangent of the rotation angle (i.e., 1% rotation indicates that the tangent of the rotation angle is 0.01).

Table 1 describes the footing properties for each of the sixteen experiments. All the properties presented in this table are in model scale and scaling laws for centrifuge tests are described in Garnier et al. (2007). All the footings in the present study were founded on medium dense sand with a relative density of 80%. They were also designed to carry similar bearing pressures of approximately 210 kPa. The parameter t_w represents the thickness of the web for the I-shaped footings. The parameter D represents the embedment of the footing and $A_c/A = \rho_{ac}$. The test name is composed of 4 segments describing: the ratio $M/(V \cdot L)$, foundation embedment, shape of the footing and the b/L ratio. As an example, the test name 1.4_e_R_0.6 reflects an embedded (e), rectangular footing (R), with $b/L = 0.6$ and

$M/V \cdot L = 1.4$. The test name 1.5_s_I35_0.13 reflects a surface (s), I-shaped footing of MAR = 35% (I35), with b/L = 0.13 and $M/(V \cdot L) = 1.5$. The eight footings that were embedded had $A_c/A \approx 0.1$ and the eight surface footings had $A_c/A \approx 0.3$. The results of these 16 experiments on sand are analyzed along with the test data analyzed by Johnson (2012) and are presented in the following section.

TEST RESULTS

INITIAL ROCKING STIFFNESS

As shown in Figure 2b, the rocking stiffness (K_{50}) represents the stiffness of the footing along line AF. ASCE 41-13 suggests conventional elastic solutions by Gazetas (1991) using the expected shear modulus and Poisson's ratio to obtain the initial stiffness of the uncoupled rotational springs. The technique proposed by Johnson (2012) for obtaining the parameter g (rotation to mobilize rocking capacity) was used to evaluate the rocking stiffness by fitting the experimental moment-rotation hysteresis data with the proposed trilinear backbone curve. For each test, the corresponding experimental rocking moment capacity was also measured and a matrix of K_{50} and $M_{c\text{-}foot}$ was obtained. Figure 3a plots the experimental rocking stiffness (K_{50} using Johnson's technique) versus the rocking stiffness obtained from ASCE 41-13 equations (K_{yy}). The results show that the ASCE 41-13 equations consistently overestimate K_{50}. The equations based upon elastic theory are more accurate for small rotation demands as they neglect the soil yielding and are used mainly for the elastic range. However, the experimental K_{50} was obtained at point F, where $f = 0.5$ and $M = 0.5M_{c\text{-}foot}$. At this point, we expect some yielding and footing uplift to have occurred, leading to a reduction in the stiffness. If the experimental rocking stiffness was calculated at a smaller rotation, the results

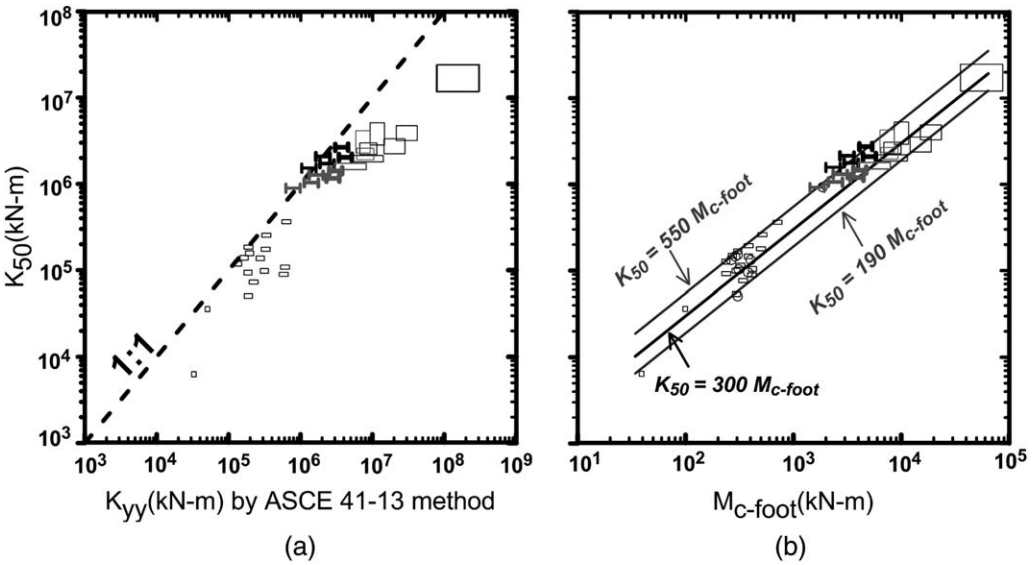

Figure 3. (a) Measured K_{50} vs. ASCE 41-13 method, (b) measured K_{50} vs. measured $M_{c\text{-}foot}$.

from the two methods would be more similar. Deng et al. (2014) observed that the stiffness, K_{50}, was approximately proportional to the rocking moment capacity when 50% of the capacity is mobilized, and that the ratio K_{50}/M_{c-foot} ranged from 230 to 460. For design of rectangular rocking footings, they suggested that $K_{50} \approx 300\,M_{c\text{-}foot}$. Figure 3b plots the measured K_{50} and the $M_{c\text{-}foot}$ values from the data generated by Johnson (2012) and the MAHS test series. It is noted that about 68% of the data points (mean plus/minus one standard deviation) lie between the $K_{50}/M_{c\text{-}foot}$ ratios of 190 and 550. As it will be shown later, I-shaped footings with a larger MAR were found to have larger $K_{50}/M_{c\text{-}foot}$ ratios than other footings.

The parameter h/2 is used to describe the rotation at point F in Figure 2b. Therefore, the parameter h can be deduced as the ratio of $M_{c\text{-}foot}/K_{50}$ (i.e., $1/h = K_{50}/M_{c\text{-}foot}$). Deng et al. (2014) proposed a value of 0.0033 for parameter h which is consistent with their recommendation of the ratio $K_{50}/M_{c\text{-}foot}$ for rectangular footings to be approximately 300 ($1/h = 1/300 = 0.0033$). To investigate the stiffness to strength ratio $K_{50}/M_{c\text{-}foot}$ further, an attempt was made to see if this ratio could be correlated to the ratio of stiffness/strength for the soil, G/q_c, where G is the soil's shear modulus and q_c is the ultimate bearing capacity of the critical contact area. One of the methods in ASCE 41-13 for determination of the shear modulus of sandy soils is given by Equation 5a:

$$G_0 = 435(N_1)_{60}^{1/3}\sqrt{P_a\sigma'_{mp}} \tag{5a}$$

In this equation $(N_1)_{60}$ is the Standard Penetration Test blow count corrected to an equivalent hammer energy efficiency of 60%, and an overburden of 1 atmosphere. For our centrifuge tests, the blow count was obtained from $(N_1)_{60} = C_d(D_R^2)$. According to Idriss and Boulanger, the value of C_d may vary in the range of 35 (e.g., laboratory samples) to 55 (e.g., natural deposits). An intermediate value ($C_d = 46$) was used for this paper, although a marginally better correlation would be observed in Figure 3a if a lower value of C_d (e.g., $C_d = 35$ for laboratory samples) had been adopted. The parameter σ'_{mp} is the mean effective stress averaged over the relevant region below the footing. ASCE 41-13 suggests obtaining this value as the larger value of Equation 5a and σ'_{v0}, where σ'_{v0} is the effective vertical stress at a depth of $(D + 0.5B)$. In Equation 5b, Q is the expected bearing load on the footing, including load due to overburden soil above the footing:

$$\sigma'_{mp} = \frac{1}{6}\left(0.52 - 0.04\frac{L}{B}\right)\frac{Q}{A} \tag{5b}$$

Figure 4 plots the correlation between $K_{50}/M_{c\text{-}foot}$ and G/q_c. Figure 4a plots this correlation for embedded footings with $0.09 < \rho_{ac} < 0.14$ and Figure 4b plots this correlation for surface footings with $0.2 < \rho_{ac} < 0.5$. Due to the narrow footing width across the flange or web, and the sensitivity of bearing capacity to the width of a footing for shallow foundations on sand, the I-shaped footings in sand will mobilize at a smaller ultimate bearing capacity pressure (q_c) than a rectangular footing of similar length and width. Furthermore, the I-shaped section has a larger moment of inertia than a rectangular shape of the same area, hence, one might expect the rotational stiffness to be greater for an I-shape than for a rectangular shape. Therefore, we expect the ratio G/q_c and $K_{50}/M_{c\text{-}foot}$ to be larger for

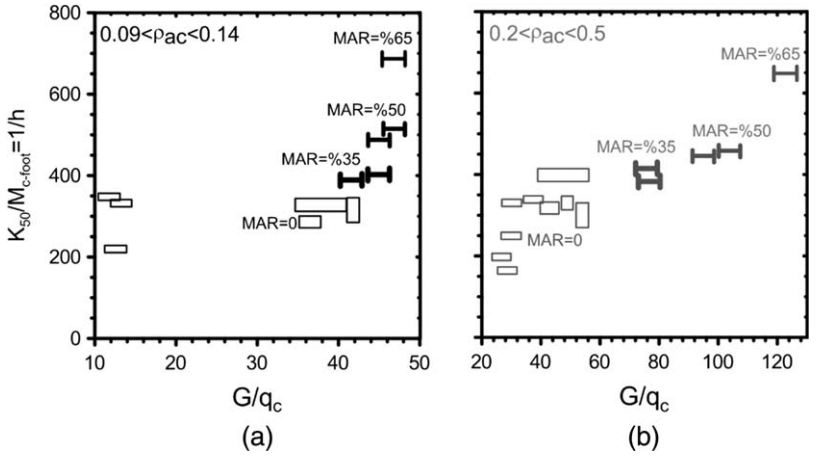

Figure 4. Correlation between $K_{50}/M_{c\text{-}foot}$ vs. G/q_c for (a) embedded, small ρ_{ac} footings and (b) surface, large ρ_{ac} footings.

the I-shaped footings than rectangular footings of similar initial embedment and bearing pressure. As the MAR increases, we also expect these ratios to increase accordingly. In Figure 4, the shapes of the data point symbols represent the geometry of the corresponding footings. Results show that for most rectangular footings ($MAR = 0$), the proposed value of $K_{50}/M_{c\text{-}foot} = 300$ by Deng et al. (2014) is a good fit, regardless of the value of ρ_{ac}. This ratio ranges from 150–450 for different shapes of rectangular footings. The very-long-narrow footing ($b/L = 0.14$) seems to have the highest ratio between all the rectangular footings, for both ranges of ρ_{ac}. For I-shaped footings, as the MAR increases, the ratio of G/q_c and the ratio $1/h = K_{50}/M_{c\text{-}foot}$ increase accordingly. For an I-shaped footing with $MAR = 65\%$, $1/h \approx 700$ while for an I-shaped with $MAR = 35\%$, $1/h \approx 400$. The small range of $K_{50}/M_{c\text{-}foot}$ for a wide range of footing sizes and shapes may be unexpected.

ROTATION TO MOBILIZE CAPACITY, *g*

As introduced in ASCE 41-13 and shown in Figure 2b, the parameter g is the rotation to mobilize the rocking moment capacity. ASCE 41-13 proposes different g values based on the footing's ρ_{ac} (Table 8-4 in ASCE 41-13, excerpts of which are provided in Kutter et al. 2016). For rectangular footings, the parameter g does not vary with footing shape for similar ρ_{ac} values. However, for I-shaped footings of the same ρ_{ac}, the standard anticipates a variation of g with MAR. For footings which lie between the proposed values, linear interpolation is permitted by the standard. Deng et al. (2014) and Johnson (2012) recommended the use of $g = 0.012$ for design of rocking rectangular footings if $\rho_{ac} \approx 1/8$. Figure 5 compares the experimental g values versus the interpolated ASCE 41-13 values for footings of the same shape and ρ_{ac}. The experimental results include the data from the sixteen MAHS test series (Table 1) as well as the data analyzed by Johnson (2012).

For rectangular footings, the interpolated ASCE 41-13 values fit reasonably with the experimental results. For the very-long-narrow footing ($b/L = 0.14$), the difference is larger

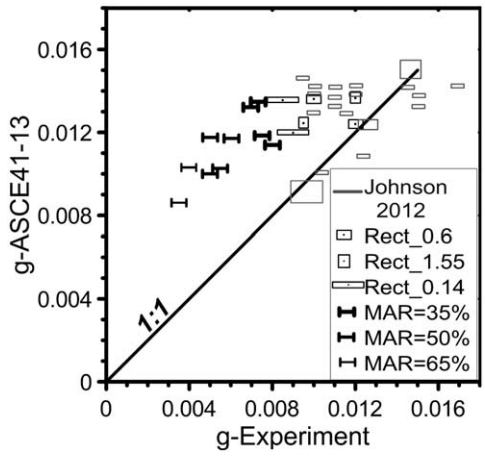

Figure 5. Rotation to mobilize capacity from ASCE 41-13 and experiments.

than for the other shapes of rectangular footings. In beam bending theory, the magnitude of the strain hardening after yielding at the extreme fiber of a beam is larger for a rectangular section than an I-shaped section. For an I-shaped section, as the flange area is fully plastified, and the section does not strengthen much due to the relatively small width of the web. For a rectangular section, the shape of the stress distribution is not expected to undergo a sudden change. Similar to beam theory, as an I-shaped footing leaves the linear range, the flange of the footing plastifies and goes into the nonlinear range. For footings of smaller flange thickness (larger MAR), a smaller rotation demand is needed to mobilize the rocking capacity as we expect a faster plastification of the entire flange area. Although the experimental results and the standard agree in the decreasing pattern in g with increasing MAR, it appears that ASCE 41-13 overestimates the g parameter for the I-shaped footings by approximately a factor of 1.5. As shown by Deng et al. (2014), determination of this parameter directly affects the magnitude of the hysteretic damping. They showed that as g decreases, the ratio $K_{50}/M_{c\text{-}foot}$ increases, yielding an increase in the hysteretic damping.

COMPARISON OF TEST RESULTS TO ASCE 41-13 BACKBONE CURVE

From the component action table for nonlinear procedures (Table 8-4 in ASCE 41-13 and Table 1 in Kutter et al. 2016), linear interpolation was used to obtain the modeling parameters and the allowable rotation demands for the sixteen footings tested; values interpolated from the table are summarized in Table 2. In addition to the parameters listed in Table 2, the method proposed by Deng et al. (2014) is used for the unloading segment (line CZ in Figure 2b) and shown in Figures 6 and 7. The unloading lines from Deng et al. (2014), described more in the next section of this paper, are shown commencing from the IO, and LS acceptance limits listed in Table 2. The CP limit point is also indicated in Figures 6 and 7. The experimental hysteretic response is shown in gray, with the black ASCE 41-13 backbone curve superimposed. The ASCE 41-13 backbone curve generally captures the overall shape of the measured hysteretic response.

Table 2. Modeling parameters and acceptance criteria for the tested footings based on ASCE 41-13

Test Name	g (rad.)	d (rad.)	f	IO (rad.)	LS (rad.)	CP (rad.)
1.4_e_R_0.6	0.0124	0.1	0.5	0.0134	0.0674	0.0842
1.45_e_R_1.55	0.0124	0.1	0.5	0.0157	0.0800	0.1000
1.57_e_R_0.14	0.0118	0.1	0.5	0.0111	0.0486	0.0607
1.5_e_I50_0.11	0.0100	0.1	0.5	0.0098	0.0393	0.0491
1.5_e_I50_0.17	0.0102	0.1	0.5	0.0092	0.0382	0.0478
1.5_e_I35_0.13	0.0114	0.1	0.5	0.0105	0.0433	0.0541
1.5_e_I35_0.26	0.0117	0.1	0.5	0.0096	0.0417	0.0522
1.5_e_I65_0.09	0.0086	0.1	0.5	0.0091	0.0368	0.0460
2_s_R_1.55	0.0136	0.1	0.5	0.0093	0.0477	0.0597
1.6_s_R_0.14	0.0135	0.1	0.5	0.0060	0.0319	0.0400
1.4_s_R_0.6	0.0136	0.1	0.5	0.0074	0.0383	0.0480
1.5_s_I35_0.26	0.0133	0.1	0.5	0.0049	0.0236	0.0296
1.5_s_I35_0.13	0.0133	0.1	0.5	0.0047	0.0228	0.0286
1.5_s_I50_0.17	0.0117	0.1	0.5	0.0042	0.0179	0.0225
1.5_s_I50_0.11	0.0117	0.1	0.5	0.0042	0.0179	0.0225
1.5_s_I65_0.09*	0.0103*	0.1*	0.5*	0.0032*	0.0112*	0.0141*

* The b/L_c for this scenario is 0.7 and ASCE 41-13 does not have recommended modeling parameters for $b/L_c < 1$. The interpolated values assume $b/L_c = 1$.

It is instructive to compare the magnitude of the rotation to mobilize the moment capacity (g) to the allowable total footing rotation for various performance points. For the IO performance level, this may be done by comparing columns "IO" and "g" in Table 2 or graphically in Figures 6 and 7. For the footings with low $\rho_{ac} = A_c/A$ (the embedded footings for this test program), the allowable IO rotation is comparable to g for I-shaped footings and narrow rectangular footings rocking in the strong direction. For the embedded rectangular footings with larger widths, the IO rotation is somewhat greater than g. For the footings with larger ρ_{ac} (surface footings for this test program), the allowable IO rotation is substantially less than g, especially for narrow rectangular footings and I-shaped footings rocking in the strong direction; this is consistent with the known trend that the potential for residual settlement increases for narrow and I-shaped footings that are rocking in the strong direction. This trend is discussed in more detail in the following sections.

In some of the graphs in Figure 6 and 7 (especially the last graph for the I-shaped footing with 65% missing area ratio) the moment capacity changes somewhat noticeably over the course of the cycling. This is primarily attributed to changes in overburden associated with residual settlement or uplift of the footings. As the foundation settles or uplifts, the surcharge term in the bearing capacity formula will change, leading to a different A_c and ρ_{ac}. For foundations with larger expected settlements (or uplifts), this change is more pronounced as the change in the surcharge term becomes more significant. It can be shown that the change in the rocking moment capacity is not very sensitive to the change in the surcharge term and ρ_{ac};

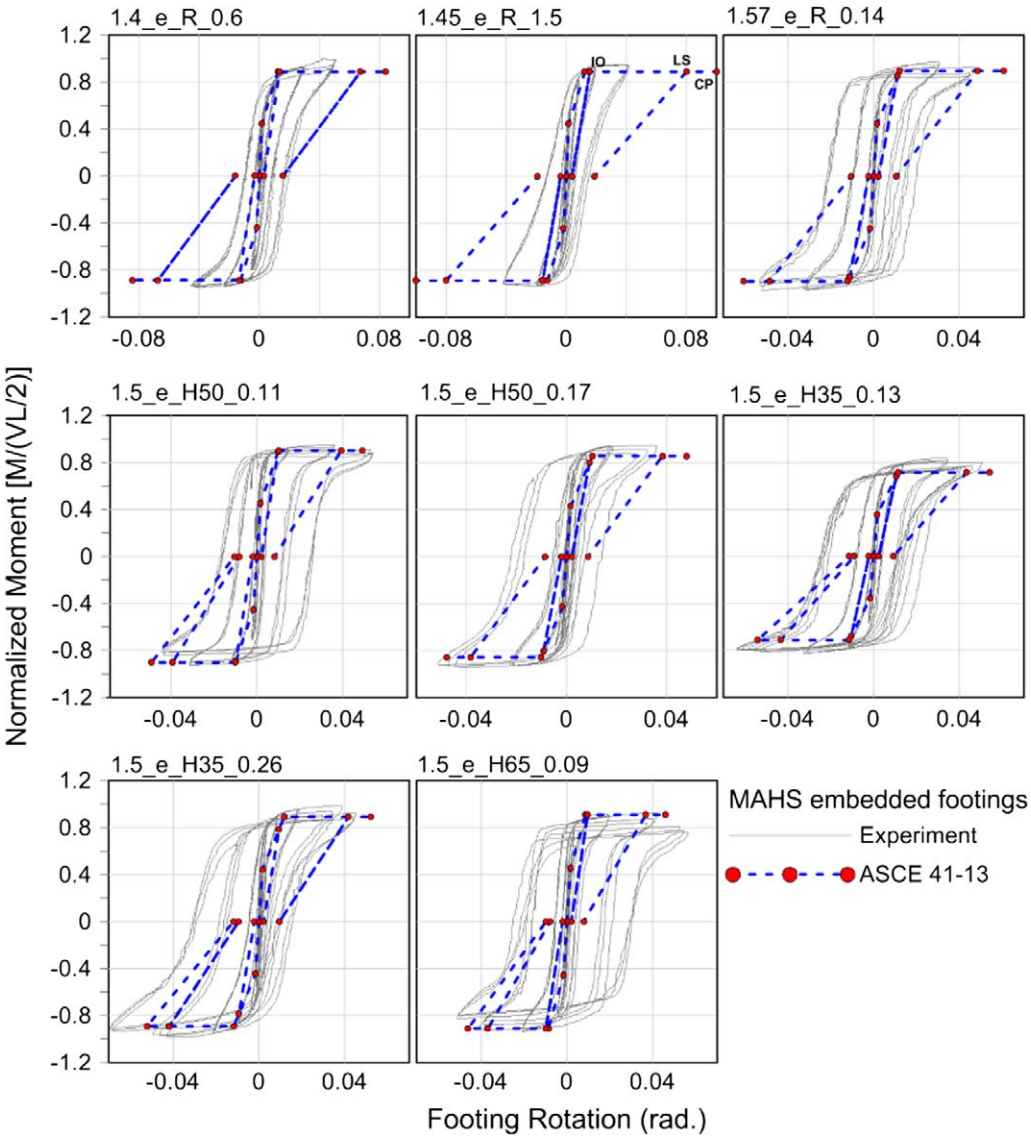

Figure 6. ASCE 41-13 backbone curves for MAHS embedded footings with data points corresponding to modeling parameters f, g, and acceptance limits IO, LS, and CP. Two unloading lines are shown for each graph, one commencing from the allowable IO rotation and one from LS.

the degradation in capacity is negligible for rotations less than the LS limit. As shown in Equation 2, if ρ_{ac} is small, the rocking moment capacity is approximately proportional to P and L and is insensitive to ρ_{ac}. As an example, if the bearing capacity changes ρ_{ac} from 0.2 to 0.1, the final rocking moment capacity will only be changed by 10%.

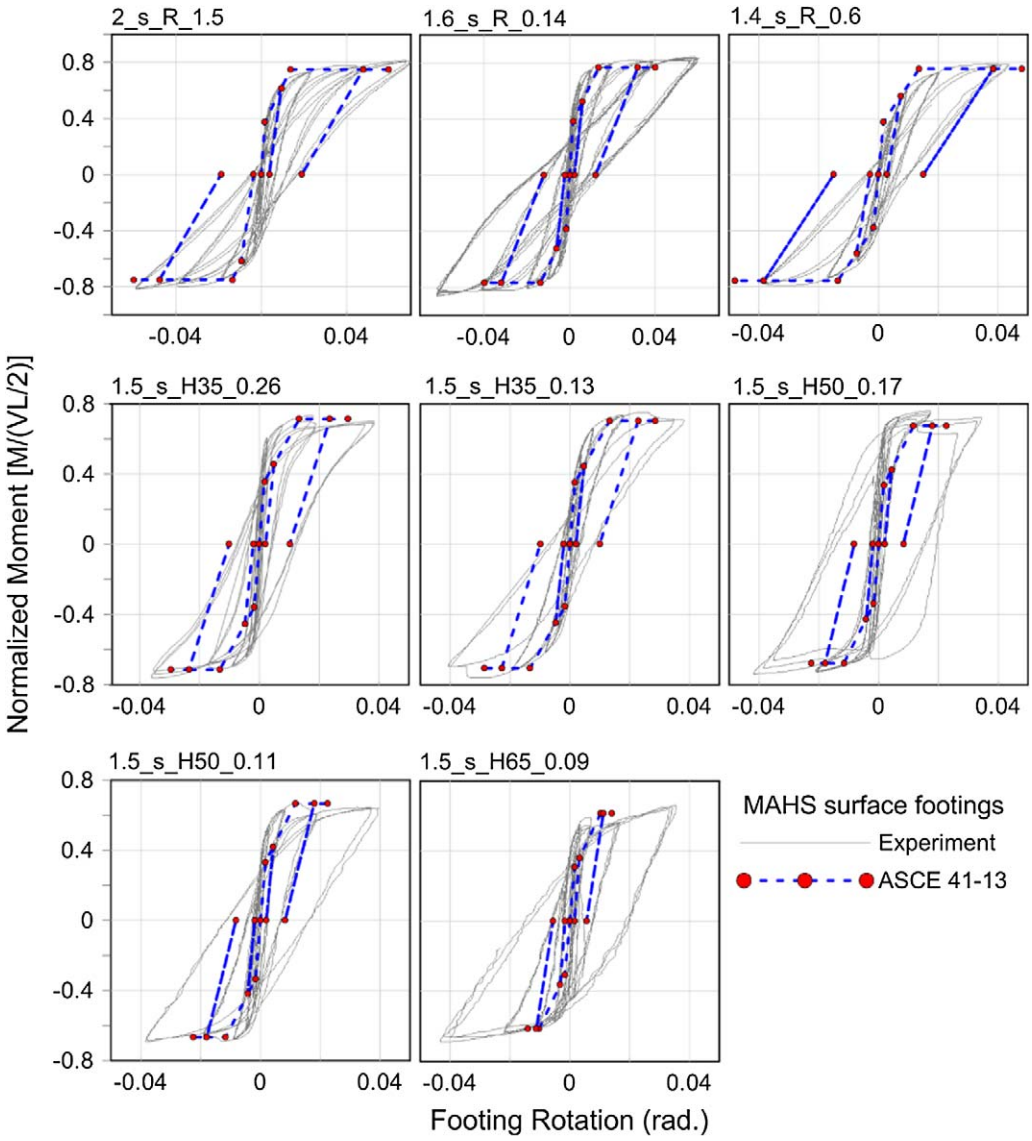

Figure 7. ASCE 41-13 backbone curves for MAHS surface footings with data points corresponding to modeling parameters f, g, and acceptance limits IO, LS, and CP. Two unloading lines are shown for each graph, one commencing from the allowable IO rotation and one from LS.

RE-CENTERING RATIO, R_d

The re-centering capability of a rocking footing (R_d) is not directly accounted for in ASCE 41-13, but re-centering is one of the positive attributes of the rocking mechanism. Hence, we have attempted to quantify the effects in this section. Deng et al. (2014) defined the re-centering ratio as:

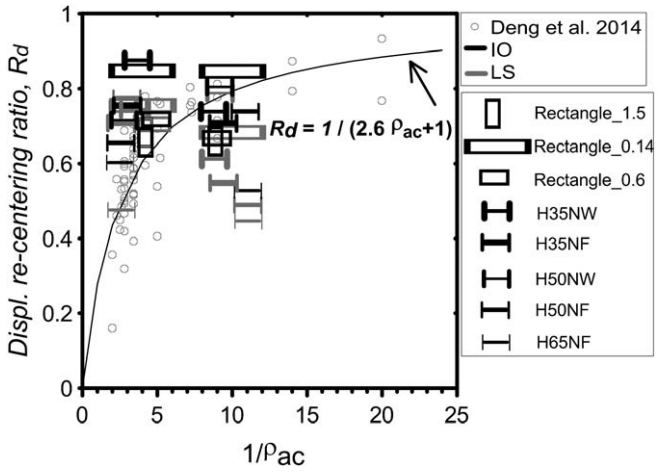

Figure 8. Empirical correlation between R_d vs. $1/\rho_{ac}$.

$$R_d = 1 - \frac{z}{d} \tag{6}$$

In this equation, z is the residual rotation of the footing upon unloading (moment = 0) and the parameter d is the maximum footing rotation for the corresponding hysteresis loop. The re-centering mechanism of a rocking footing is largely a result of the gap closure as the moment is released. If the foundation was rocking on a rigid surface, ($1/\rho_{ac}$ = infinite), we would expect a perfect re-centering, leading to $R_d = 1$ (i.e., $z = 0$). On the other hand, if the axial load (P) was exactly equal to the foundation's bearing capacity (i.e., $1/\rho_{ac} = 1$), we expect no re-centering to occur since no gap is formed as the foundation rotates; this situation would give $z \approx d$ and $R_d \approx 0$. Based on data available at the time, Deng et al. (2014) proposed an empirical correlation for R_d with respect to the foundation's critical contact area ratio (ρ_{ac}), as shown in Equation 7.

$$R_d = \frac{1}{2.6\rho_{ac} + 1} \tag{7}$$

The re-centering ratios (R_d) of the footings listed in Table 1 are calculated for the IO and LS acceptance rotations. These data points, along with the data from Deng et al. (2014), are plotted in Figure 8. The existing data are shown in lighter gray color circles while the new data points are in bold lines and the symbols used represent the shape of the footings tested. Furthermore, the unloading lines for these computed re-centering ratios have been added to Figures 6 and 7. The results depicted in Figure 6 (embedded footings) show an over-estimation of the re-centering ratio by the Deng et al. (2014) correlation, especially for the LS & CP levels. Equation 7 suggests that re-centering improves as ρ_{ac} decreases, which is correct, but in addition, the re-centering ability is diminished if soil material falls into the gap that opens up under the footing during rocking. The data points in Figure 8 near $\rho_{ac} = 0.1$ ($1/\rho_{ac} = 10$) are for embedded footings in dry sand where sand easily ravels into the gap; for these footings Equation 7 overestimates re-centering. For surface footings (the group of data points near

$\rho_{ac} = 0.3$ in this study, shown in Figure 7) where soil material will not ravel into the gap, Equation 7 conservatively estimates the re-centering.

It should also be pointed out that the re-centering ratio depends on the amplitude of rotation, where R_d tends to decrease as rotation demand increases. This can be seen in that the gray data points (subsequent to LS rotation) are lower than the black points (subsequent to IO rotation). Figure 8 results reveal that the surface and embedded very-long-narrow footings (1.57_e_R_0.14 & 1.6_s_R_0.14), denoted as Rectangle_0.14, demonstrate a relatively large re-centering ratio. As shown in Table 2, the acceptance limits for the long-narrow footing is smaller than that of other rectangles of same ρ_{ac}. Therefore, the higher re-centering of a very-long-narrow footing is solely attributed to the decreased rotation for the IO and LS acceptance limits. Despite all of these issues, with the exception of the embedded I-shaped footing of $MAR = 65\%$ (1.5_e_I65_0.09), the correlation seems to reasonably capture the re-centering capability of the footings. The surface I-shaped footing of $MAR = 65\%$ (1.5_s_I65_0.09) exerts the lowest re-centering capability for both IO and LS levels due to the least lateral confinement around the rocking edge. The re-centering ratio for the I-shaped and rectangular footings rocking in the strong direction 1.5_s_I65_0.09, 1.6_s_R_0.14, and 1.5_s_I35_0.26 show a clear drop from IO to the LS rotation angle.

FOUNDATION SETTLEMENT AND UPLIFT FOR THE LEVELS OF ACCEPTANCE CRITERIA

Cumulative settlement is one of the primary potential detrimental aspects of rocking foundations. It is well known that permanent deformations, especially settlement, can accumulate with every cycle of rocking. It has been well documented (Gajan et al. 2008, Hakhamaneshi and Kutter 2016, Hakhamaneshi et al. 2012 and Deng et al. 2014) that if the ρ_{ac} is large (e.g., greater than 0.2 or so), settlement can become significant. In an attempt to examine the suitability of the acceptance criteria, the amount of permanent settlement (or uplift) right before and after exceeding each acceptance limit is examined. Figure 9a shows an

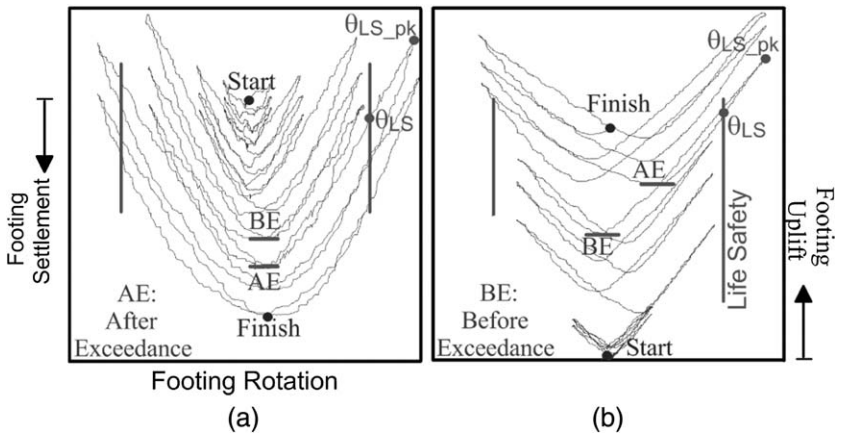

Figure 9. Permanent settlement before (BE) and after exceeding (AE) Life Safety acceptance criteria rotation for (a) a surface footing that settles, and (b) an embedded footing that uplifts.

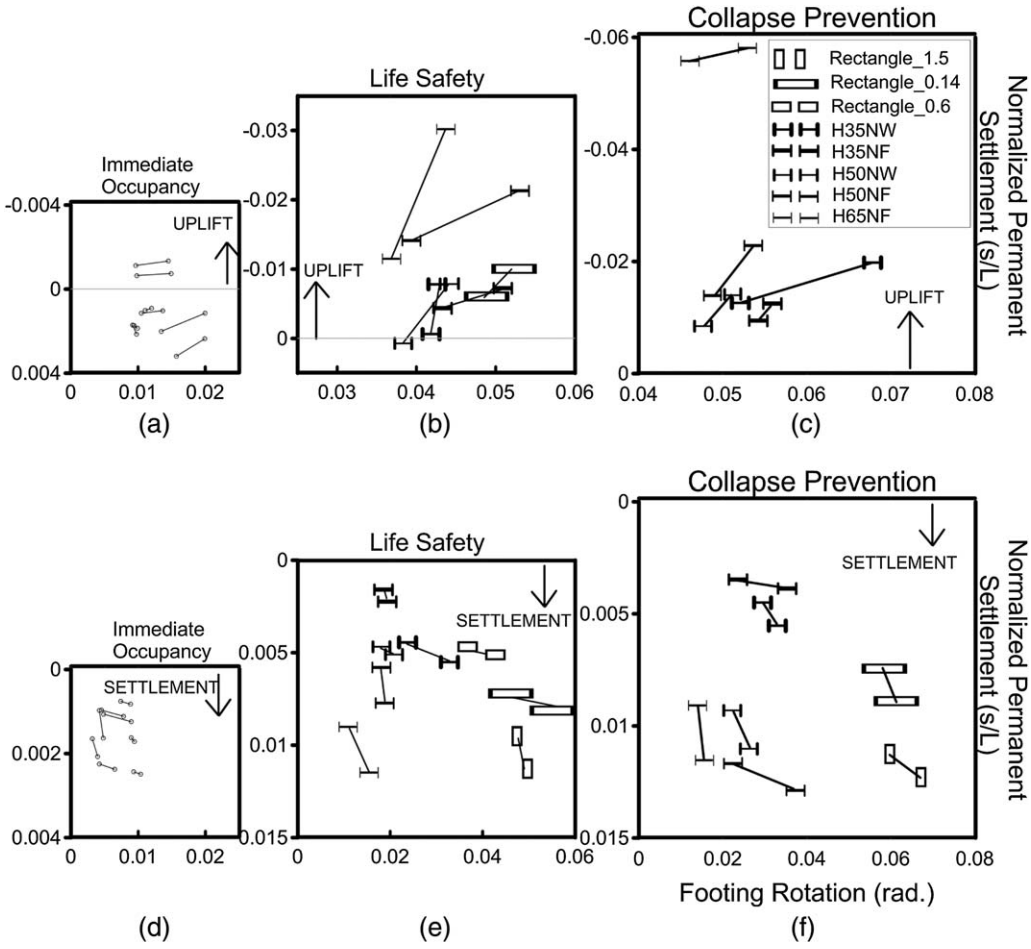

Figure 10. Normalized permanent settlement vs. footing rotation for MAHS embedded (a, b, and c) and surface (d, e, and f) footings. Note that negative permanent settlement indicates permanent uplift. Two connected data points are shown per test—one just before and one just after exceeding the acceptance criteria.

example relationship between the footing settlement and the footing's rotation for a surface footing in the present study and Figure 9b shows a similar relationship for an embedded footing that exhibits residual uplift. The LS acceptance criteria for this particular footing, θ_{LS}, is indicated by a vertical line while the peak footing rotation for the first cycle that exceeds this limit is denoted as $\theta_{LS\text{-}pk}$. The residual settlement or uplift corresponding to this peak in rotation is measured by the local minimum in the uplift attained during unloading and reloading in the opposite direction. These local minima before (BE) and after exceeding (AE) the acceptance criteria are indicated in the legend of Figure 9. This process was repeated for all of the footings and for each of the IO, LS, and CP acceptance limits with the results presented in Figure 10. These figures plot the normalized permanent

uplift/settlement for the IO, LS, and CP acceptance limits, and for the embedded/surface footings, accordingly.

As shown in Figure 10a, the magnitude of normalized permanent settlement or uplift for all the embedded footings at the IO level, is smaller than 0.4% of *L*. In Figure 10b, prior to exceeding the LS rotation demand, the magnitude of normalized permanent uplift is smaller than 1.5% of *L*. In Figure 10c, with the exception of the embedded I-shaped footing of MAR = 65% (1.5_e_I65_0.09), the amount of normalized permanent uplift remains smaller than 2% of L. In the future revisions to the ASCE 41-13 standard, the allowable footing rotation for the embedded I65 footing (1.5_e_I65_0.09) could be reduced to about 3% to produce settlements consistent with other footings. As shown in Figure 10 (d, e, and f), the normalized permanent settlement of all the surface footings for the IO, LS & CP acceptance limits, remains smaller than 0.4%, 1.3% and 1.5% of *L*, respectively. The proposed values seem to limit the footing settlement to reasonable values for each level of acceptance criteria.

CONCLUSIONS

This study describes some background associated with the modeling parameters and acceptance criteria for the nonlinear static and dynamic procedures in the updated standard ASCE 41-13 *Seismic Evaluation and Retrofit of Existing Buildings*. A trilinear backbone curve is used to model the hysteretic moment-rotation behavior of a rocking shallow foundation. The method proposed by Deng et al. (2014) for estimating the re-centering of a rocking footing is used to complete the loading-unloading-reloading shape of the backbone curve. ASCE 41-13 adopts the use of elasticity solutions based upon Gazetas (1991) to obtain the rocking stiffness (K_{yy}). These formulas are mainly based on the shear modulus of the soil under the footing which is non-uniform and difficult to accurately determine. A simpler method for obtaining the stiffness, $K_{50} = 300M_{c\text{-}foot}$, is proposed for rectangular footings. For I-shaped footings, it is found that K_{50} varies from $400M_{c\text{-}foot}$ to $700M_{c\text{-}foot}$. The direct correlation between moment capacity and K_{50} appears to be a promising practical and reasonably accurate method for determining the secant stiffness of a rocking foundation for the point at which half of the moment capacity is mobilized.

Results from a series of 16 centrifuge tests on embedded and surface rocking footings are presented. The moment-rotation behavior in these tests compare favorably to the proposed backbone curve in ASCE 41-13. The proposed re-centering method by Deng et al. (2014) overestimates the re-centering effects for embedded footings in dry sand, as it does not completely take into account the effect of sand raveling into the gap formed under a rocking footing. The ASCE 41-13 acceptance criteria are evaluated by studying the amount of permanent settlement (and uplift) immediately before and after exceeding each level of acceptance criteria (IO, LS, and CP). Except for embedded I-shaped footings of large missing area ratio (MAR), the proposed values reasonably limit the permanent settlement to the corresponding levels of acceptance criteria.

The rotation to mobilize the rocking capacity (g) is obtained for the 16 experiments and the results are compared to the previously published results by Deng et al. (2014). It is found that rectangular footings mobilize the capacity at a rotation of approximately 0.012 radians. As expected, I-shaped footings are found to mobilize the capacity at a smaller rotation

demand. I-shaped footings of largest MAR mobilize the capacity fastest as the web of the footing does not contribute significantly to the moment capacity. While the ASCE 41-13 standard proposes a reduction in the g parameter as MAR increases, further reduction is recommended to better match the experimental values for footings with a large MAR.

ACKNOWLEDGMENTS

This work was primarily supported by NSF-NEESR under Grant number CMMI 0936503. Any findings, statements and conclusions are those of the authors, and do not necessarily reflect the opinions of the sponsoring organizations. The authors would like to thank the suggestions and contributions of Prof. Sashi Kunnath, Prof. Tara C. Hutchinson, Prof. Ross Boulanger, Prof. Mark Aschheim, Dr. Weian Liu, and Andreas G. Gavras.

REFERENCES

Allotey, N., and El Naggar, M. H., 2008. An investigation into the Winkler modeling of the cyclic response of rigid footings, *Soil Dyn. Earthq. Eng.* **28**, 44–57.

Anastasopoulos, I., Gazetas, G., Loli, M., Apostolou, M., and Gerolymos, N., 2010. Soil failure can be used for seismic protection of structures, *Bull. Earthq. Eng.* **8**, 309–326.

American Society of Civil Engineers (ASCE), 2014. *Seismic Evaluation and Retrofit of Existing Buildings* (ASCE/SEI 41-13), Reston, VA.

Deng, L., Kutter, B. L., and Kunnath, S., 2012a. Centrifuge modeling of bridge systems designed for rocking foundations, *J. Geotech. Geoenviron. Engrg.*, DOI: 10.1061/(ASCE)GT .1943-5606.0000605.

Deng, L., and Kutter, B. L., 2012b. Characterization of rocking shallow foundations using centrifuge model tests, *Earthquake Engng. Struct. Dyn.* **41**, 1043–1060, doi: 10.1002/eqe .1181.

Deng, L., Kutter, B., and Kunnath, S., 2014. Seismic design of rocking shallow foundations: displacement-based methodology, *J. Bridge Eng.*, Applied Technology Council (ATC), 2011. *Quantification of Building Seismic Performance Factors: Component Equivalency Methodology, FEMA P-795,* prepared for the Federal Emergency Management Agency, Redwood City, CA. 10.1061/(ASCE)BE.1943-5592.0000616.

Gajan, S., and Kutter, B. L., 2008. Capacity, settlement, and energy dissipation of shallow footings subjected to rocking, *J. Geotech. Geoenviron. Engrg.*, ASCE, **134**, 1129–1141.

Garnier, J., Gaudin, C., Springman, S. M., Culligan, P. J., Goodings, D. J., Konig, D., Kutter, B. L., Phillips, R., Randolph, M. F., and Thorel, L., 2007. Catalogue of scaling laws and similitude questions in geotechnical centrifuge modeling, *International Journal of Physical Modelling in Geotechnics* **7**, 1–23.

Gazetas, G., 1991. Foundation vibrations. *Foundation Engineering Handbook* (H. Y. Fang, Editor), Van Nostrand Reinhold, New York.

Hakhamaneshi, M., Kutter, B. L., Deng, L., Hutchinson, T. C., and Liu, W., 2012. New findings from centrifuge modeling of rocking shallow foundations in clayey ground, *Proceedings of ASCE 2012 Geo-congress*, 25–29 March 2012, Oakland, CA.

Hakhamaneshi, M., 2014. Rocking Foundations for Building Systems, Effect of Footing Shape, Soil Environment, Embedment and Normalized Moment-to-Shear Ratio, Ph.D. Thesis, University of California, Davis, CA.

Hakhamaneshi, M., and Kutter, B. L., 2016. Effect of footing shape and embedment on the settlement, recentering and energy dissipation of shallow footings subjected to rocking, *J. Geotech. Geoenviron. Engrg.*, ASCE, in press.

Idriss, I. M., and Boulanger, R. W., 2008. *Soil Liquefaction during Earthquakes*, EERI MNO-12, Earthquake Engineering Research Institute, Oakland, CA, 235 pp.

Johnson, K. E., 2012. Characterization of Test Results of Rocking Shallow Foundations Using a Multi-Linear Hysteretic Model, M.S. Report, University of California, Davis, CA.

Kutter, B. L., Moore, M., Hakhamaneshi, M., and Champion, C., 2016. Rationale for shallow foundation rocking provisions in ASCE 41-13, *Earthquake Spectra* **32**, 1097–1119.

Liu, W., Hutchinson, T. C., Kutter, B. L., Hakhamaneshi, M., Aschheim, M., and Kunnath, S., 2013. Demonstration of compatible yielding between soil-foundation and superstructure components, *Journal of Structural Engineering*, ASCE, **139**, 1408–1420.

Liu, W., Hutchinson, T. C., Kutter, B. L., Gavras, A. G., and Hakhamaneshi, M., 2015. Seismic behavior of frame-wall-rocking foundation systems-Part I: Test program and slow cyclic test results, *Journal of Structural Engineering*, ASCE, in press.

Meyerhof, G.G., 1963. Some recent research on the bearing capacity of foundations, *Can. Geotech. J.* **1**, 16–26.

(Received 19 December 2014; accepted 27 July 2015)